Inorganic Chemistry

Article

pubs.acs.org/IC

Color-Tunable and White Luminescence Properties via Energy Transfer in Single-Phase $KNaCa_2(PO_4)_2$:A (A = Ce^{3+}, Eu^{2+}, Tb^{3+}, Mn^{2+}, Sm^{3+}) Phosphors

Dongling Geng,[†,‡] Mengmeng Shang,[†] Yang Zhang,[†,‡] Hongzhou Lian,[†] and Jun Lin*[,†]

[†]State Key Laboratory of Rare Earth Resource Utilization, Changchun Institute of Applied Chemistry, Chinese Academy of Sciences, Changchun 130022, People's Republic of China

[‡]University of Chinese Academy of Sciences, Beijing 100049, People's Republic of China

Supporting Information

ABSTRACT: A series of single-phase phosphors based on $KNaCa_2(PO_4)_2$ (KNCP):A (A = Ce^{3+}, Eu^{2+}, Tb^{3+}, Mn^{2+}, Sm^{3+}) have been prepared via the Pechini-type sol–gel method. Photoluminescence (PL) and cathodoluminescence (CL) properties of Ce^{3+}-, Eu^{2+}-, Tb^{3+}-, Mn^{2+}-, and Sm^{3+}-activated KNCP phosphors were investigated. For the A singly doped KNCP samples, they exhibit the characteristic emissions of the A activator. Na^+ ions exhibit the best charge compensation result among Li^+, Na^+, and K^+ ions for Ce^{3+}-, Tb^{3+}-, and Sm^{3+}-doped KNCP samples. The energy transfers from Ce^{3+} to Tb^{3+} and Mn^{2+} ions as well as Eu^{2+} to Tb^{3+} and Mn^{2+} have been validated. The emission colors of KNCP:Ce^{3+}/Eu^{2+}, Tb^{3+}/Mn^{2+}, Na^+ samples can be adjusted by energy transfer process and changing the Tb^{3+}/Mn^{2+} concentration. More importantly, white light emission in KNCP:Eu^{2+}, Mn^{2+} system has been obtained. The KNCP:Tb^{3+}, Na^+ sample shows tunable luminescence from blue to cyan and then to green with the change of Tb^{3+} concentration due to the cross-relaxation from $^5D_3$ to $^5D_4$. A white emission can also be realized in the single-phase KNCP host by reasonably adjusting the doping concentrations of Tb^{3+} and Sm^{3+} (reddish-orange emission) under low-voltage electron beam excitation. Additionally, the temperature-dependent PL properties of as-prepared phosphors reveal that the KNCP host has good thermal stability. Therefore, the KNCP:A (A = Ce^{3+}, Eu^{2+}, Tb^{3+}, Mn^{2+}, Sm^{3+}) phosphors could be regarded as good candidates for UV W-LEDs and FEDs.

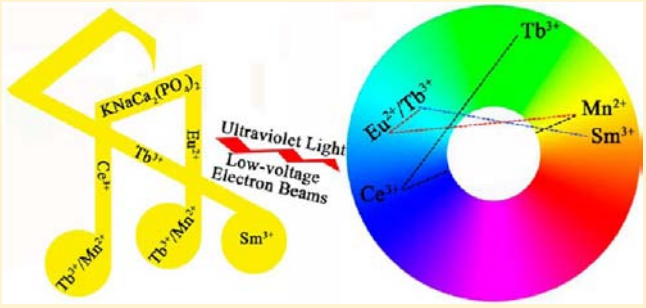

1. INTRODUCTION

White light-emitting diodes (W-LEDs) and field emission displays (FEDs) have drawn much research attention in recent years.[1] Among various phosphor-converted (pc) W-LEDs, the shortcomings for a W-LED that was obtained by combining yellow phosphor YAG:Ce and a blue InGaN chip are a bad color rendering index (Ra < 80) and high color temperature (T_c > 7000 K) because of the absence of red composition, blocking its extension to more fascinating applications.[2] To bypass this headache, it is practicable to achieve white light emission by employing several phosphors with UV LED chips.[3] However, poor luminous efficiency attributed to the reabsorption among phosphors is another challenging problem. Thus, to develop phosphors that can produce white emission in the single phase becomes an urgent task.[4] On the other hand, the available phosphors for FEDs cannot adapt to the harsh operation conditions perfectly.[5] Consequently, new phosphors with high quality need to be developed to meet the demand of LEDs and FEDs. In addition, the Pechini sol–gel method is a useful and convenient technique to prepare inorganic non-metallic materials.[6] It has many advantages compared with the conventional solid-state reaction, such as homogeneous mixing of the starting materials at the molecular level and low synthetic temperature, good control of stoichiometry, fine particle size, and uniform morphology.[7]

In this Article, we report the synthesis of $KNaCa_2(PO_4)_2$ (KNCP):A (A = Ce^{3+}, Eu^{2+}, Tb^{3+}, Mn^{2+}, Sm^{3+}, and their combinations, in some cases) phosphors using the Pechini-type sol–gel method. According to a previous report, there are at least two different crystallographic sites in the KNCP host.[8] The broad band emissions of Ce^{3+}, Eu^{2+}, and Mn^{2+} ions at different sites in the KNCP host are investigated in this study. Na^+ ions exhibit the strongest charge compensation ability among Li^+, Na^+, and K^+ ions for Ce^{3+}-, Tb^{3+}-, and Sm^{3+}-doped KNCP samples. Additionally, the energy transfer properties from Ce^{3+}/Eu^{2+} to Tb^{3+}/Mn^{2+} under UV and low-voltage electron beam excitation were investigated and are discussed in detail. More interestingly, white light emission in the KNCP:Eu^{2+}, Mn^{2+} system has been obtained by energy transfer and changing the relative doping concentrations of activators. Furthermore, a white emission can also be realized in the

Received: September 11, 2013
Published: November 4, 2013

   dx.doi.org/10.1021/ic402305x | Inorg. Chem. 2013, 52, 13708–13718

single-phase KNCP host by controlling the doping concentrations of Tb^{3+} and Sm^{3+} under low-voltage electron beam excitation. In summary, the as-prepared single-phase-based KNCP phosphors show wide-range-tunable blue, green, reddish-orange, and white emissions under UV and low-voltage electron beam excitation, which has potential applications in W-LEDs and FEDs.

2. EXPERIMENTAL SECTION

2.1. Materials. Eu_2O_3, Tb_4O_7, and Sm_2O_3 (99.999%) were purchased from Science and Technology Parent Company of Changchun Institute of Applied Chemistry, and other chemicals were purchased from Beijing Chemical Company. All chemicals were of analytical grade and used directly without further purification.

2.2. Preparation. A series of polycrystalline KNCP and different concentrations of Ce^{3+}, Eu^{2+}, Tb^{3+}, Mn^{2+}, and Sm^{3+} ion-doped KNCP phosphors were prepared by the Pechini-type sol−gel method. The $Li^+/Na^+/K^+$ ions were used as charge compensators for Ce^{3+}, Tb^{3+}, and Sm^{3+} ion-doped KNCP samples. Typically, stoichiometric amounts of Eu_2O_3, Tb_4O_7, and Sm_2O_3 were dissolved in dilute nitric acid (HNO_3) under stirring and heating, resulting in the formation of a colorless solution of $Eu(NO_3)_3$, $Tb(NO_3)_3$, and $Sm(NO_3)_3$, respectively. First, stoichiometric amounts of $Ca(NO_3)_2{\cdot}4H_2O$, $Ce(NO_3)_3{\cdot}6H_2O$, $Mn(CH_3COO)_2$, $LiNO_3/NaNO_3/KNO_3$, and the solution of $Eu(NO_3)_3$, $Tb(NO_3)_3$, and $Sm(NO_3)_3$ were mixed together, stirring for 15 min; then citric acid was dissolved in the above solution (citric acid/metal ion = 2:1 in moles). The pH of the solution was adjusted to ∼1 with HNO_3 followed by the addition of stoichiometric amounts of $KH_2(PO_4)_2$ and $NaH_2(PO_4)_2$. Finally, a certain amount of deionized water was added into the above solution until the volume was 30 mL, and 3 g of polyethylene glycol (PEG, molecular weight = 20 000, A.R.) was added as a cross-linking agent (C_{PEG} = 0.01 mol/L) after stirring for 10 min. The resultant mixtures were stirred for 2 h and then heated at 75 °C in a water bath until homogeneous gels formed. After prefiring at 500 °C for 4 h in air, the samples were fully ground and calcined at 950 °C in air for 4 h. The obtained Ce^{3+}- and Eu^{2+}-related powders were then reduced at 900 °C for 4 h under a 5% H_2/95% N_2 atmosphere to produce the final samples.

2.3. Characterization. The X-ray diffraction (XRD) measurements were carried out on a D8 Focus diffractometer using Cu Kα radiation (λ = 0.15405 nm). The photoluminescence (PL) measurements were performed on a Hitachi F-7000 spectrophotometer equipped with a 150 W xenon lamp as the excitation source. The temperature-dependent (300−500 K) PL spectra were obtained on a fluorescence spectrophotometer equipped with a 450 W xenon lamp as the excitation source (Edinburgh Instruments, FLSP-920) with a temperature controller. The CL measurements were carried out in an ultrahigh-vacuum chamber (<10^{-8} Torr), where the phosphors were excited by an electron beam in the voltage range 2.5−5.0 kV and different filament currents, and the emission spectra were recorded using an F-7000 spectrophotometer. Photoluminescence absolute quantum yields (QYs) were measured by an absolute PL quantum yield measurement system (C9920-02, Hamamatsu Photonics K. K., Japan). The luminescence decay curves were obtained from a Lecroy Wave Runner 6100 digital osilloscope (1 GHz) using a tunable laser (pulse width = 4 ns, gate = 50 ns) as the excitation (Contimuum Sunlite OPO) source.

3. RESULTS AND DISCUSSION

3.1. Phase and Crystal Structure. Figure 1 shows the representative XRD patterns for KNCP:0.04Ce^{3+}, 0.04Na^+, KNCP:0.01Eu^{2+}, KNCP:0.05Tb^{3+}, 0.05Na^+, KNCP:0.04Ce^{3+}, 0.05Tb^{3+}, 0.09Na^+, KNCP:0.04Ce^{3+}, 0.05Mn^{2+}, 0.04Na^+, and KNCP:0.008Eu^{2+}, 0.08Mn^{2+} samples. It is obvious that the diffraction peaks of all these samples are in good agreement with the JCPDS Standard Card no. 51-0580 of $KNaCa_2(PO_4)_2$,

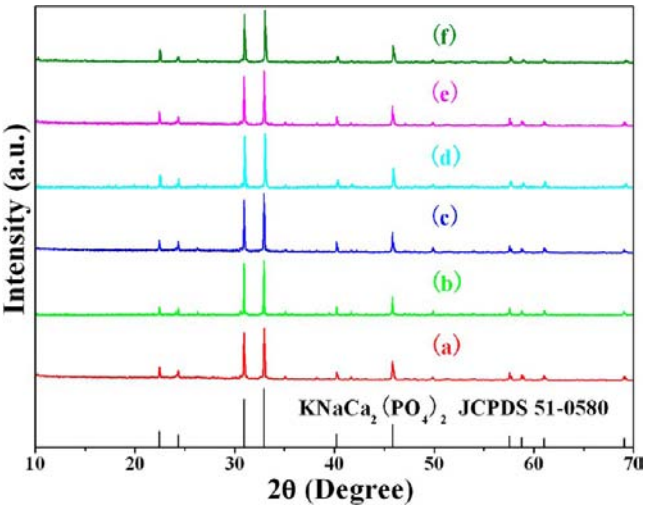

Figure 1. XRD patterns for KNCP:0.04Ce^{3+}, 0.04Na^+ (a), KNCP:0.01Eu^{2+} (b), KNCP:0.05Tb^{3+}, 0.05Na^+ (c), KNCP:0.04Ce^{3+}, 0.05Tb^{3+}, 0.09Na^+ (d), KNCP:0.04Ce^{3+}, 0.05Mn^{2+}, 0.04Na^+ (e), and KNCP:0.008Eu^{2+}, 0.08Mn^{2+} (f).

indicating that the obtained samples are single phase and adopt the same structure as $KNaCa_2(PO_4)_2$. According to the XRD patterns, we can deduce that the Ce^{3+}, Eu^{2+}, Tb^{3+}, Mn^{2+}, and Na^+ ions were completely dissolved in the KNCP host without inducing significant changes of the crystal structure.

3.2. PL Properties of $Ce^{3+}/Eu^{2+}/Tb^{3+}/Mn^{2+}/Sm^{3+}$ Singly Doped KNCP Samples. *KNCP:Ce^{3+}, Na^+.* Figure 2a shows the

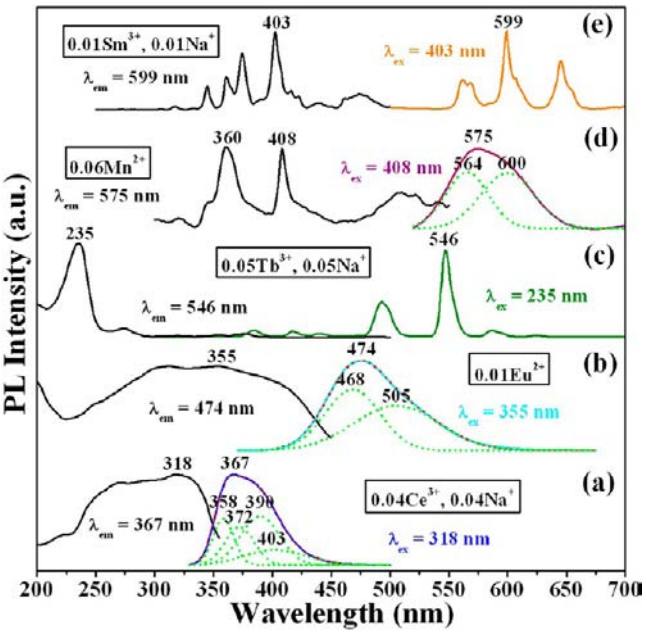

Figure 2. Excitation (left) and emission (right) spectra for KNCP:0.04Ce^{3+}, 0.04Na^+ (a), KNCP:0.01Eu^{2+} (b), KNCP:0.05Tb^{3+}, 0.05Na^+ (c), KNCP:0.06Mn^{2+} (d), and KNCP:0.01Sm^{3+}, 0.01Na^+ (e).

excitation and emission spectra of the KNCP:0.04Ce^{3+}, 0.04Na^+ sample. The excitation spectrum (black line) of KNCP:0.04Ce^{3+}, 0.04Na^+ monitored at 367 nm shows a broad band in the region from 230 to 350 nm, which can be attributed to the transitions from the ground state to the different crystal field splitting levels of the 5d state for Ce^{3+} ions in the KNCP

dx.doi.org/10.1021/ic402305x | Inorg. Chem. 2013, 52, 13708−13718

host. Figure S1 gives the diffuse reflection spectra of KNCP (black line) and KNCP:0.04Ce^{3+}, 0.04Na^+ (red line) samples, which were recorded in the spectrum region from 200 to 550 nm at room temperature. The undoped KNCP host has a broad absorption band from 200 to 350 nm. As Ce^{3+} ions were doped into the KNCP host, a strong absorption in the range 240−360 nm assigned to the 4f → 5d absorption of Ce^{3+} ions was observed.[9] The absorption band in the diffuse reflection spectra and the excitation spectrum of KNCP:0.04Ce^{3+}, 0.04Na^+ matched well. The emission spectrum (blue line in Figure 2a) exhibits an asymmetric emission band with a maximum at about 367 nm when excited by 318 nm UV. Generally, the Ce^{3+}-emission spectrum has doublet character because of the spin−orbit splitting of the ground state ($^2F_{5/2}$ and $^2F_{7/2}$) with an energy difference of about 2000 cm^{-1}.[10] However, the emission band of KNCP:0.04Ce^{3+}, 0.04Na^+ can be decomposed into four well-separated Gaussian components with peak centers at 358, 372, 390, and 403 nm. Clearly, these four peaks can arise from not only the ground state splitting but also the different Ce^{3+} centers. Wang et al. have given the coordination environments for the two crystallographic sites of Ca^{2+} ions in the KNCP host calaulated by the van Uitert formula: eight and six coordination centers.[8] Figure 2Sa and b display the energy level diagrams of Ce^{3+} at the two different coordination fields. From the van Uitert formula and the energy level diagrams,[11] we can conclude that the two bands centered at 358 and 390 nm (energy difference is about 2292 cm^{-1}) are attributed to the Ce^{3+} ions entering the eight-coordinated center, and the two bands located at 372 and 403 nm (energy difference is about 2068 cm^{-1}) are due to the emission of Ce^{3+} ions occupying the six-coordinated center.

In the KNCP crystallite, Ce^{3+} ions are expected to replace Ca^{2+} sites. However, it would be difficult to maintain a charge balance in the samples. Therefore, univalent ions (Li^+, Na^+, or K^+) were added as charge compensators in order to keep the charge balance. It is worth mentioning that the charge compensators $Li^+/Na^+/K^+$ for Ce^{3+}-doped KNCP samples also substitute the Ca^{2+} site and the doping concentration of the charge compensators $Li^+/Na^+/K^+$ is equal to that of Ce^{3+}. So the doped charge compensators $Li^+/Na^+/K^+$ would not transform the composition of the KNCP host, although it is composed of Na^+ and K^+. Figure S3a shows the charge compensation effect of different charge compensators on the emission intensity of the KNCP:0.02Ce^{3+} phosphor. It is found that all three charge compensators increase the emitting intensity of KNCP:0.02Ce^{3+}. Obviously, Na^+ ions exhibit the best charge compensation result among Li^+, Na^+, and K^+ ions. The order of charge compensation abilities is $Na^+ > K^+ > Li^+$. This result may be attributed to the ionic radius size of Li^+, Na^+, K^+, and Ca^{2+}. Compared with the radius of Li^+ and K^+ ions, the Na^+ ionic radius is more similar to that of Ca^{2+}. Na^+ as charge compensator together with Ce^{3+} substituted two Ca^{2+} sites in the KNCP crystal lattice, which would lead to a smaller lattice deformation than Li^+ and K^+,[12] so the KNCP:0.02Ce^{3+}, 0.02Na^+ phosphor shows the strongest luminescence intensity. Similarly, the radius of the K^+ ion is closer to that of the Ca^{2+} ion than the Li^+ ion. Thus KNCP:0.02Ce^{3+}, 0.02K^+ shows stronger luminescence intensity than KNCP:0.02Ce^{3+}, 0.02Li^+.

The PL intensity of Ce^{3+} as a function of its doping concentration (x) in the KNCP:$x$$Ce^{3+}$, $x$$Na^+$ sample is shown in Figure S4a. The PL intensity reaches a maximum value at x = 0.04, then decreases with further increase of its concentration due to the concentration quenching effect.[13] Thus, the optimum doping concentration for Ce^{3+} in the KNCP host is 4 mol % of Ca^{2+}.

KNCP:Eu^{2+}. The excitation and emission spectra of KNCP:0.01Eu^{2+} are shown in Figure 2b. The excitation spectrum has a broad hump between 230 and 440 nm, which is attributed to the $4f^7 \rightarrow 4f^65d^1$ transition of the Eu^{2+} ions. The broad excitation band matches well with the range of the near-UV LED chip (380−420 nm),[14] and the absorption band shown in the diffuse reflection spectrum of KNCP:0.01Eu^{2+} (green line in Figure S1) is consistent with its excitation spectrum. Under 355 nm UV excitation, the KNCP:0.01Eu^{2+} phosphor emits blue-green light in the range 420−550 nm, which can be attributed to the typical $4f^65d^1 \rightarrow 4f^7$ transition of Eu^{2+} ions. By Gaussian deconvolution, the PL spectrum of the KNCP:0.01Eu^{2+} phosphor can be decomposed into two Gaussian bands with peaks centered at 468 and 505 nm, respectively. The splitting bands can be ascribed to different emission sites in the KNCP host. The emission band centered at 468 nm originates from the Eu^{2+} center of the eight-coordinated site, and the band centered at 505 nm originates from the Eu^{2+} center of the six-coordinated site. The energy level diagrams of Eu^{2+} in the eight- and six-coordinated fields shown in Figure S2c and d can give us a clear delineation. This observation can be confirmed by previous literature, which also reported the splitting bands in the KNCP:Eu^{2+} sample.[8] The relative emission intensity dependence on the doping concentration of Eu^{2+} ions (m) is presented in Figure S4b. The optimal doping concentration of Eu^{2+} in the KNCP host is m = 0.008.

KNCP:Tb^{3+}, Na^+. Figure 2c shows the excitation and emission spectra of the KNCP:0.05Tb^{3+}, 0.05Na^+ sample. The excitation spectrum monitored with the characteristic green emission (546 nm) of Tb^{3+} includes several lines in the region from 300 to 450 nm and a broad band peaking at about 235 nm. The broad band is ascribed to the spin-allowed transition from the 4f to the 5d state of the Tb^{3+} ion, whereas the sharp lines correspond to absorption due to the forbidden f−f transition of the Tb^{3+} ion. The weak band at 274 nm corresponds to the spin-forbidden transition of the Tb^{3+}.[15] The diffuse reflection spectrum of the KNCP:0.05Tb^{3+}, 0.05Na^+ sample presented in Figure S1 (blue line) shows a broad absorption band in the range 220−270 nm, which corresponds to the $4f^8 - 4f^75d$ spin-allowed transition in the excitation spectrum. It is clear that the KNCP:Tb^{3+}, Na^+ phosphor can be optimally excited at 235 nm UV. The emission spectrum of KNCP:0.05Tb^{3+}, 0.05Na^+ consists of the $^5D_{3,4} \rightarrow {}^7F_J$ transitions of Tb^{3+} ions. In fact, many Tb^{3+}-activated materials show blue emission from the $^5D_3$ level and green emission from the $^5D_4$ level.[16] The energy difference between $^5D_3$ and $^5D_4$ is close to that between $^7F_0$ and $^7F_6$, which sometimes corresponds to the energy transfer of identical centers: $^5D_3$ (Tb^{3+}) + $^7F_6$ (Tb^{3+}) → $^5D_4$ (Tb^{3+}) + $^7F_0$ (Tb^{3+}).[17] The emission spectra show different ratios between the $^5D_3$ and the $^5D_4$ emissions with the increase of Tb^{3+} concentration, as shown in Figure 3a. In the emission spectra for low doping concentrations (y < 0.01), the $^5D_3 \rightarrow {}^7F_J$ transitions are dominant, and, the $^5D_4 \rightarrow {}^7F_5$ transition at 546 nm is dominant at higher doping concentrations (y > 0.01). The emission intensities of $^5D_3 \rightarrow {}^7F_J$ and $^5D_4 \rightarrow {}^7F_J$ transitions with respect to the doping concentration of Tb^{3+} ions (y) are presented in Figure 3b. When y = 0.008 and 0.08 mol, the $^5D_3 \rightarrow {}^7F_J$ and $^5D_4 \rightarrow {}^7F_J$ emissions reach their maximum intensities, respectively. The cross-relaxation between the $^5D_3$−$^5D_4$ and $^7F_0$−$^7F_6$ of the two neighboring Tb^{3+}

dx.doi.org/10.1021/ic402305x | Inorg. Chem. 2013, 52, 13708−13718

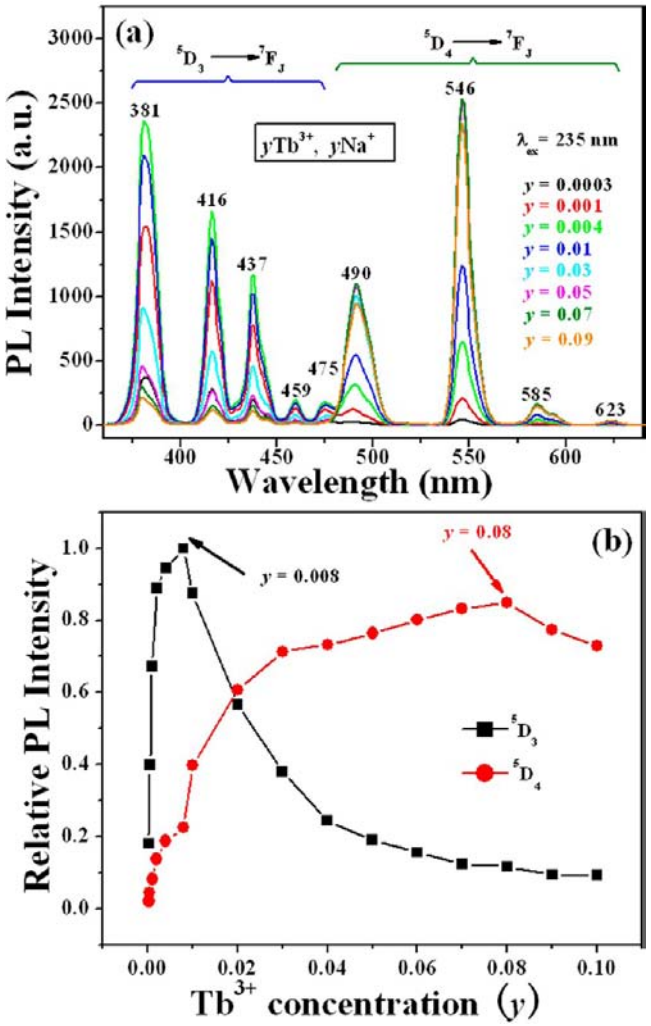

Figure 3. Emission spectra for KNCP:yTb^{3+}, yNa$^+$ with different Tb^{3+} concentrations (a) and the emission intensities of $^5D_3$ and $^5D_4$ in KNCP:yTb^{3+}, yNa$^+$ samples as a function of y (b).

ions results in the quenching of the blue emissions of $^5D_3 \rightarrow {}^7F_J$ transitions. The emissions of the $^5D_4 \rightarrow {}^7F_J$ transitions are quenched by the energy migration among the activators.

Similar to KNCP:Ce^{3+} phosphors, the univalent ions Li$^+$, Na$^+$, and K$^+$ were also added as charge compensators in the KNCP:0.05Tb^{3+} sample (Figure S3b in the Supporting Information). The experimental results indicate that Na$^+$ is the optimum charge compensator for the KNCP:Tb^{3+} sample, which in line with that in the KNCP:Ce^{3+} sample. Therefore, we chose Na$^+$ ions as the charge compensators for Ce^{3+}-, Tb^{3+}-, and Sm^{3+}-doped KNCP phosphors.

KNCP:Mn^{2+}. The excitation and emission spectra of KNCP:0.06Mn^{2+} are shown in Figure 2d. The excitation spectrum consists mainly of two peaks located at 360 and 408 nm, corresponding to the transitions from $^6A_1$ (^6S) to $^4T_2$ (^4D) and [$^4A_1$ (^4G), ^4E (^4G)] of Mn^{2+}, respectively.[18] The diffuse reflection spectrum of KNCP:0.06Mn^{2+} shown in Figure S1 (cyan line) is almost identical with that of the host (black line) below 350 nm. However, two small absorption bands at 360 and 409 nm have been detected, which can be supported by the excitation spectrum. Under 408 nm light excitation, the broad and asymmetric emission band centered at 575 nm is attributed to the spin-forbidden $^4T_1$ (^4G) $\rightarrow$ $^6A_1$ (^6S) transition of Mn^{2+}.[18] Clearly, the emission band can be decomposed into two Gaussian bands centered at 546 and 600 nm, respectively. We can infer that Mn^{2+} ions occupied two different emission sites in the KNCP host. The energy level diagrams of Mn^{2+} in crystal fields are similar to that of Eu^{2+}, which are also shown in Figure S2c and d. Therefore, the eight-coordinated Mn^{2+} site is responsible for the 546 nm emission band, and the six-coordinated Mn^{2+} site is responsible for the 600 nm emission band. According to Figure S4c in the Supporting Information, the best doping concentration of Mn^{2+} in the KNCP host is z = 0.06.

KNCP:Sm^{3+}, Na$^+$. The black line plotted in Figure 2e shows the excitation spectrum of the KNCP:0.01Sm^{3+}, 0.01Na$^+$ phosphor, which is composed of several peaks at 345 nm ($^6H_{5/2} \rightarrow {}^4K_{17/2}$), 361 nm ($^6H_{5/2} \rightarrow$ (^4D, ^6P)$_{15/2}$), 375 nm ($^6H_{5/2} \rightarrow {}^4L_{17/2}$), 403 nm ($^6H_{5/2} \rightarrow {}^4K_{11/2}$), and 474 nm ($^6H_{5/2} \rightarrow {}^4I_{13/2}$), respectively.[19] Among them, $^6H_{5/2} \rightarrow {}^4K_{11/2}$ is the strongest excitation band at 403 nm. The diffuse reflection spectrum of the KNCP:0.01Sm^{3+}, 0.01Na$^+$ sample is shown in Figure S1 (pink line). The broad absorption band in the range 220−340 nm is attributed to the absorption of the KNCP host, and the weak absorption peaks at 363, 376, 404, and 476 nm correspond to the f−f transition of the Sm^{3+} ions. Under 403 nm UV excitation, KNCP:0.01Sm^{3+}, 0.01Na$^+$ gives emissions at 562, 599, and 645 nm, which correspond to the transitions from $^4G_{5/2}$ to $^6H_{5/2}$, $^6H_{7/2}$, and $^6H_{9/2}$ of Sm^{3+}, respectively.[19] From Figure S4d in the Supporting Information, we can note that the emission intensity of KNCP:tSm^{3+}, tNa$^+$ reaches its maximum when t = 0.02.

3.3. Energy Transfer Properties. *KNCP:Ce^{3+}, Tb^{3+}/Mn^{2+}, Na$^+$*. Generally, the Ce^{3+} ions can act as an efficient sensitizer by transferring its excitation energy to coactivators.[20] In the KNCP:Ce^{3+}, Tb^{3+}/Mn^{2+}, Na$^+$ system, the Ce^{3+} ions can serve as an effective sensitizer for Tb^{3+} or Mn^{2+}, which not only help Tb^{3+} and Mn^{2+} ions to emit efficiently but also tune the emission color of the co-doped samples.

Figure 4a and c show excitation spectra for KNCP:0.04Ce^{3+}, 0.06Tb^{3+}, 0.1Na$^+$ and KNCP:0.04Ce^{3+}, 0.07Mn^{2+}, 0.04Na$^+$ samples, respectively. For the KNCP:0.04Ce^{3+}, 0.06Tb^{3+}, 0.1Na$^+$ sample, the excitation spectrum monitored with the Tb^{3+} $^5D_4 \rightarrow {}^7F_5$ transition (546 nm) consists of the excitation bands of both Tb^{3+} (220−240 nm) and Ce^{3+} ions (240−350 nm). The presence of the Ce^{3+} absorption band indicates that the energy transfer process from Ce^{3+} to Tb^{3+} ions exists.[21] For the KNCP:0.04Ce^{3+}, 0.07Mn^{2+}, 0.04Na$^+$ sample, the excitation spectrum monitored with the Mn^{2+} $^4T_1 \rightarrow {}^6A_1$ transition (600 nm) is almost identical with that monitored with Ce^{3+} emission (367 nm). This result means that Mn^{2+} ions are essentially excited through Ce^{3+} ions and the energy transfer process from Ce^{3+} to Mn^{2+} ions is expected in the KNCP:Ce^{3+}, Mn^{2+}, Na$^+$ system. Comparing the emission intensity of KNCP:Tb^{3+}/Mn^{2+}, Na$^+$ samples under 235 or 408 nm UV excitation with that of KNCP:Ce^{3+}, Tb^{3+}/Mn^{2+}, Na$^+$ samples under 270 nm UV excitation, we can find that the emission intensity of Tb^{3+}/Mn^{2+} ions has been enhanced remarkably by co-doping Ce^{3+} ions into the host, although the concentration of Tb^{3+}/Mn^{2+} stays unchanged (as shown in Figure S5a and b).

The emission spectra for KNCP:0.04Ce^{3+}, yTb^{3+}, (0.04+y)Na$^+$ and KNCP:0.04Ce^{3+}, zMn^{2+}, 0.04Na$^+$ with increasing Tb^{3+} and Mn^{2+} doping concentrations are shown in Figure 4b and d. Under 270 nm UV excitation, the emission spectra consist of the emission band of Ce^{3+} and Tb^{3+}/Mn^{2+} ions, which indicates that Ce^{3+} ions have transferred part of

dx.doi.org/10.1021/ic402305x | *Inorg. Chem.* 2013, 52, 13708−13718

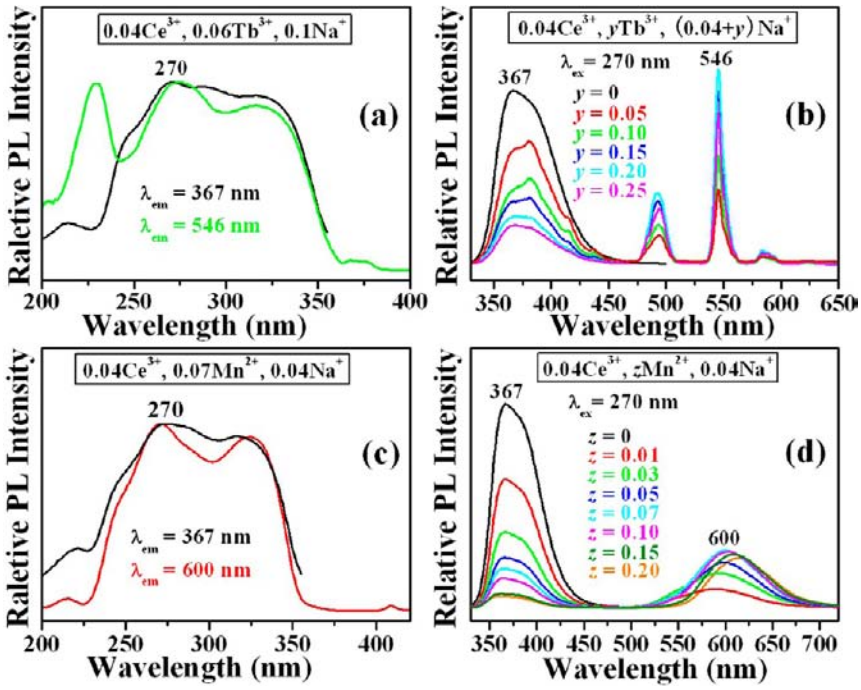

Figure 4. Excitation spectra for KNCP:0.04Ce^{3+}, 0.06Tb^{3+}, 0.1Na^{+} (a) and KNCP:0.04Ce^{3+}, 0.07Mn^{2+}, 0.04Na^{+} (c) samples. The emission spectra for KNCP:0.04Ce^{3+}, $y$$Tb^{3+}$, (0.04+$y$)$Na^{+}$ (b) and KNCP:0.04Ce^{3+}, $z$$Mn^{2+}$, 0.04$Na^{+}$ (d).

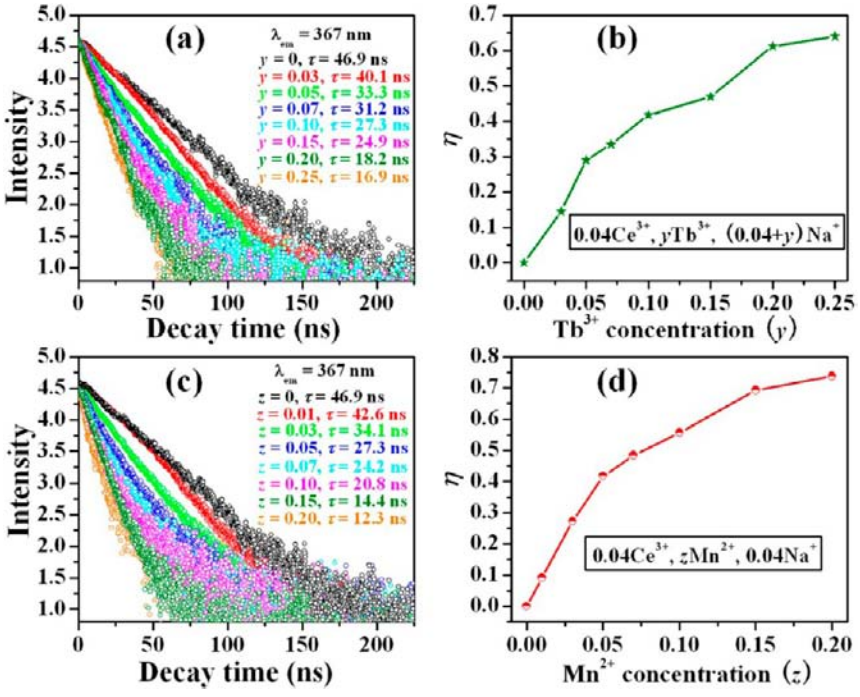

Figure 5. Decay curves for the luminescence of Ce^{3+} in KNCP:0.04Ce^{3+}, $y$$Tb^{3+}$, (0.04+$y$)$Na^{+}$ (a) and KNCP:0.04Ce^{3+}, $z$$Mn^{2+}$, 0.04$Na^{+}$ (c) samples with different Tb^{3+}/Mn^{2+} doping concentrations. The dependence of the energy transfer efficiency η on y (b) and z (d) (λ_{ex} = 270 nm).

their absorbed energy to Tb^{3+}/Mn^{2+} ions. Although the concentration of Ce^{3+} was fixed, the emission intensity of Ce^{3+} decreased with increasing Tb^{3+}/Mn^{2+} concentration, while the emission intensity of Tb^{3+}/Mn^{2+} increases with an increase of its concentration. Figure S6 presents the relative emission intensity of Ce^{3+}, Tb^{3+}, and Mn^{2+} in KNCP:0.04Ce^{3+}, $y$$Tb^{3+}$, (0.04+$y$)$Na^{+}$ (a) and KNCP:0.04Ce^{3+}, $z$$Mn^{2+}$, 0.04$Na^{+}$ (b) samples with different Tb^{3+}/Mn^{2+} doping concentrations. This result reveals efficient energy transfer occurred between Ce^{3+} and Tb^{3+}/Mn^{2+} in the KNCP host. The emission intensities of Tb^{3+} and Mn^{2+} reach their maximum values at y = 0.2 and z = 0.07, respectively.

In addition, the fluorescence lifetimes (τ) of Ce^{3+} in KNCP:Ce^{3+}, Tb^{3+}/Mn^{2+}, Na^{+} samples with different Tb^{3+}/Mn^{2+} concentrations were recorded at 367 nm (λ_{ex} = 270 nm), as shown in Figure 5a and c. The decay behaviors of Ce^{3+} ions in the KNCP:Ce^{3+}, Tb^{3+}/Mn^{2+}, Na^{+} sample show a second-

dx.doi.org/10.1021/ic402305x | Inorg. Chem. 2013, 52, 13708−13718

order exponential decay mode. The fluorescence effective lifetime of Ce^{3+} ions can be estimated by the following, eq 1:[22]

$$I(t) = A_1 \exp(-t/\tau_1) + A_2 \exp(-t/\tau_2) \quad (1)$$

where $I(t)$ represents the luminescence intensity at time t. Using these parameters, the average decay times (τ) can be determined by the following formula:[22]

$$\tau = (A_1\tau_1^2 + A_2\tau_2^2)/(A_1\tau_1 + A_2\tau_2) \quad (2)$$

From eq 2, the effective lifetime values of Ce^{3+} ions were determined to be 46.9, 40.1, 33.3, 31.2, 27.3, 24.9, 18.2, and 16.9 ns for KNCP:0.04Ce^{3+}, $y$$Tb^{3+}$, (0.04+$y$)$Na^+$ samples with y = 0, 0.03, 0.05, 0.07, 0.10, 0.15, 0.20, and 0.25, respectively. In the same way, we calculated the lifetime values of Ce^{3+} ions in KNCP:0.04Ce^{3+}, $z$$Mn^{2+}$, 0.04$Na^+$ samples, which were 42.6, 34.1, 27.3, 24.2, 20.8, 14.4, and 12.3 ns for z = 0.01, 0.03, 0.05, 0.07, 0.10, 0.15, and 0.20, respectively. The decay lifetime of Ce^{3+} ions can be found to decrease with the increase of Tb^{3+}/Mn^{2+} contents, which is powerful evidence for the energy transfer from Ce^{3+} to Tb^{3+}/Mn^{2+} ions in the KNCP host. Commonly, the energy transfer efficiency (η_T) from the sensitizer to the activator could be determined by the following expression:[23]

$$\eta_T = 1 - \frac{\tau}{\tau_0} \quad (3)$$

in which τ_0 and τ are the lifetimes of the sensitizer without and with the activator, respectively. In the KNCP host, Ce^{3+} is the sensitizer and Tb^{3+}/Mn^{2+} is the activator, respectively. The energy transfer efficiencies from Ce^{3+} to Tb^{3+} and Mn^{2+} were calculated as a function of the concentrations of Tb^{3+} and Mn^{2+}, respectively, which is plotted in Figure 5b and d. The η_T increases with increasing Tb^{3+}/Mn^{2+} doping concentration in the KNCP:Ce^{3+}, Tb^{3+}/Mn^{2+}, Na^+ system, despite the fact that the increasing rate gradually decreases. The energy transfer efficiency can also be expressed by the emission intensity of the sensitizer: $\eta_T = 1 - I_S/I_{S0}$, where I_S and I_{S0} are the luminescence intensity of the sensitizer with and without the activator present.[24] From the emission intensity of Ce^{3+}, which decreased with increasing Tb^{3+}/Mn^{2+} concentration, as shown in Figure S6, we can infer that η_T is proportional to the concentration of Tb^{3+}/Mn^{2+} ions. Under 270 nm UV excitation, the maximum energy transfer efficiencies for Ce^{3+} → Tb^{3+} and Ce^{3+} → Mn^{2+} estimated by the lifetime of Ce^{3+} are 64% and 74%, respectively. Hence, we can infer that the Ce^{3+} ions can transfer their energy to Tb^{3+}/Mn^{2+} ions effectively in the KNCP host. The emission color of the KNCP:Ce^{3+}, Tb^{3+}/Mn^{2+}, Na^+ sample can be tuned by the energy transfer process. The CIE chromaticity coordinates of the KNCP:Ce^{3+}, Tb^{3+}/Mn^{2+}, Na^+ system with different Tb^{3+}/Mn^{2+} doping concentrations are shown in Figure 6a. Obviously, the emission color of KNCP:0.04Ce^{3+}, $y$$Tb^{3+}$, (0.04+$y$)$Na^+$ and KNCP:0.04Ce^{3+}, $z$$Mn^{2+}$, 0.04$Na^+$ samples can be adjusted from blue to green and from blue to reddish-orange, respectively. The absolute quantum yields of KNCP:Ce^{3+}, Tb^{3+}/Mn^{2+}, Na^+ phosphors under 270 nm UV excitation are listed in Table 1. The QY of the KNCP:0.04Ce^{3+} phosphor is 89%. When Tb^{3+}/Mn^{2+} is co-doped into the KNCP:Ce^{3+} phosphor, the QY of KNCP:Ce^{3+}, Tb^{3+}/Mn^{2+}, Na^+ decreases with the increase of Tb^{3+}/Mn^{2+} content. This may be because the luminescence efficiency of Tb^{3+}/Mn^{2+} ions is different from that of Ce^{3+} ions under 270 nm UV excitation. The maximum QYs of as-prepared

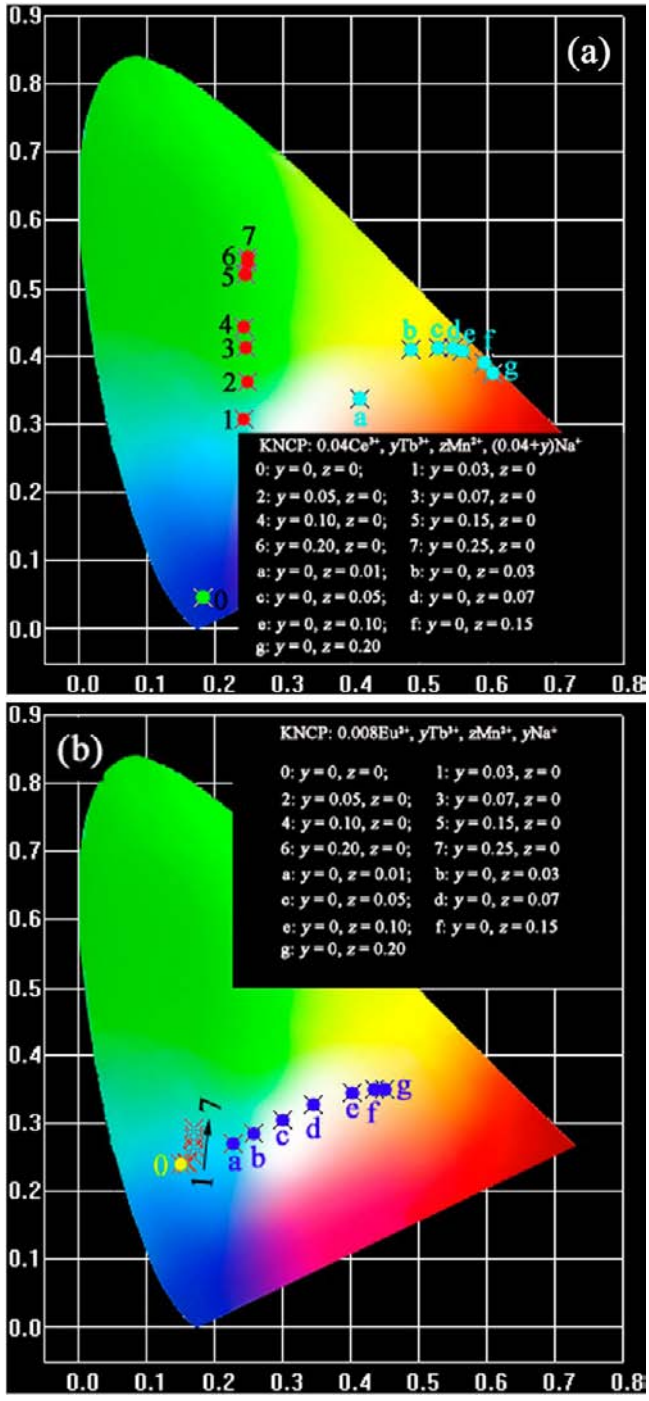

Figure 6. CIE chromaticity coordinates of KNCP:Ce^{3+}, Tb^{3+}/Mn^{2+}, Na^+ (a) and KNCP:Eu^{2+}, Tb^{3+}/Mn^{2+}, Na^+ (b) phosphors with different Tb^{3+}/Mn^{2+} doping concentrations.

KNCP:Ce^{3+}, Tb^{3+}/Mn^{2+}, Na^+ samples can reach 83% and 79% at y = 0.05 and z = 0.01, respectively. As we know, most of the current UV chips for W-LEDs are located in the range 350−420 nm. With the development of semiconductor chips, shorter UV emitting chips (250−320 nm) may be available in the future. Such technology can make phosphors used in W-LEDs that are not limited by excitation wavelength. Thus, KNCP:Ce^{3+}, Tb^{3+}/Mn^{2+}, Na^+ may have some potential applications in W-LEDs in the future.

KNCP:Eu^{2+}, Tb^{3+}/Mn^{2+}, Na^+. We also studied the luminescence and energy transfer properties of KNCP:Eu^{2+}, Tb^{3+}/

dx.doi.org/10.1021/ic402305x | Inorg. Chem. 2013, 52, 13708−13718

Table 1. Quantum Yields of KNCP:0.04Ce^{3+}, yTb^{3+}, zMn^{2+}, $(0.04+y)Na^{+}$ and KNCP:0.008Eu^{2+}, yTb^{3+}, zMn^{2+}, yNa^{+} Samples under 270 and 365 nm UV Excitation, Respectively

KNCP:0.04Ce^{3+}, yTb^{3+}, zMn^{2+}, $(0.04+y)Na^{+}$	QY	KNCP:0.008Eu^{2+}, yTb^{3+}, zMn^{2+}, yNa^{+}	QY
$y = 0, z = 0$	89%	$y = 0, z = 0$	57%
$y = 0.05, z = 0$	83%	$y = 0.05, z = 0$	38%
$y = 0.10, z = 0$	80%	$y = 0.10, z = 0$	43%
$y = 0.15, z = 0$	72%	$y = 0.15, z = 0$	41%
$y = 0.20, z = 0$	64%	$y = 0.20, z = 0$	37%
$y = 0.25, z = 0$	56%	$y = 0.25, z = 0$	33%
$y = 0, z = 0.01$	79%	$y = 0, z = 0.05$	27%
$y = 0, z = 0.05$	75%	$y = 0, z = 0.10$	31%
$y = 0, z = 0.10$	67%	$y = 0, z = 0.15$	38%
$y = 0, z = 0.15$	55%	$y = 0, z = 0.20$	37%
$y = 0, z = 0.20$	52%	$y = 0, z = 0.25$	24%

Mn^{2+}, Na^{+} samples. Besides Ce^{3+}, Eu^{2+} has been demonstrated to be another efficient sensitizer for Tb^{3+} and Mn^{2+} ions. A number of reports have been focused on the energy transfer between Eu^{2+} and Tb^{3+}/Mn^{2+}, such as $Ca_4Mg_5(PO_4)_6$:Eu^{2+}, Mn^{2+} (ref 25), $LiGd(PO_3)_4$:Eu^{2+}, Mn^{2+} (ref 26), and $KcaGd(PO_4)_2$:Eu^{2+}, Tb^{3+}, Mn^{2+} (ref 27). The excitation spectra of KNCP:0.008Eu^{2+}, 0.1Tb^{3+}, 0.1Na^{+} and KNCP:0.008Eu^{2+}, 0.07Mn^{2+} samples are shown in Figure 7a and c, respectively. Monitoring with the emission of Tb^{3+}/Mn^{2+}, the appearance of a Eu^{2+} excitation band in the excitation spectra implies that Eu^{2+} can transfer energy to Tb^{3+}/Mn^{2+} ions. From Figure S5c and d, we can know that the emission intensity of Tb^{3+}/Mn^{2+} ions could be improved by co-doping Eu^{2+} ions into KNCP:Tb^{3+}/Mn^{2+}, Na^{+} samples. The emission spectra for KNCP:0.008Eu^{2+}, yTb^{3+}, yNa^{+} and KNCP:0.008Eu^{2+}, zMn^{2+} with different concentrations of Tb^{3+} and Mn^{2+} (Figure 7b and d) illustrate the occurrence of the energy transfer from Eu^{2+} to Tb^{3+} and Mn^{2+}. With fixing the Eu^{2+} concentration at m = 0.008, the emission intensity of Eu^{2+} decreases, while that of Tb^{3+}/Mn^{2+} increases. The relative emission intensities of Eu^{2+}, Tb^{3+}, and Mn^{2+} in KNCP:0.008Eu^{2+}, yTb^{3+}, yNa^{+} and KNCP:0.008Eu^{2+}, zMn^{2+} with changing concentration of Tb^{3+}/Mn^{2+} are presented in Figure S7. When y = 0.2 and z = 0.07, the emission intensities of Tb^{3+} and Mn^{2+} reach their maximum values in KNCP:0.008Eu^{2+}, yTb^{3+}, yNa^{+} and KNCP:0.008Eu^{2+}, zMn^{2+} samples, respectively. Figure S8a and c show the decay curves for the luminescence of Eu^{2+} in KNCP:0.008Eu^{2+}, yTb^{3+}, yNa^{+} and KNCP:0.008Eu^{2+}, zMn^{2+} systems with different Tb^{3+}/Mn^{2+} doping concentrations. The luminescence decay for Eu^{2+} in both systems can be fitted with a second-order exponential. The effective lifetime values of Eu^{2+} ions in KNCP:0.008Eu^{2+}, yTb^{3+}, yNa^{+} and KNCP:0.008Eu^{2+}, zMn^{2+} samples can also be calculated with eqs 1 and 2. The decay lifetime of Eu^{2+} ions decreases with an increase in Tb^{3+}/Mn^{2+} content, proving that Eu^{2+} can transfer energy to Tb^{3+}/Mn^{2+} ions in the KNCP host. Figure S8b and d show the energy transfer efficiencies from Eu^{2+} to Tb^{3+} and Mn^{2+} calculated as a function of the concentrations of Tb^{3+} and Mn^{2+}, respectively. According to eq 3, the maximum energy transfer efficiencies for $Eu^{2+} \rightarrow Tb^{3+}$ and $Eu^{2+} \rightarrow Mn^{2+}$ can reach 70% and 76%, respectively. The emission color of KNCP:0.008Eu^{2+}, yTb^{3+}, yNa^{+} samples can be tuned predictably from blue (KNCP:0.008Eu^{2+}) with CIE chromaticity coordinates of (0.1509, 0.2389) to blue-green (KNCP:0.008Eu^{2+}, 0.25Tb^{3+}, 0.25Na^{+}) with CIE chromaticity coordinates of (0.1703, 0.2933) in the visible spectral region. Also, the emission color of KNCP:0.008Eu^{2+}, zMn^{2+} phosphors can be adjusted from blue (KNCP:0.008Eu^{2+}) through white light (KNCP:0.008Eu^{2+}, 0.07Mn^{2+}) with CIE chromaticity coordinates of (0.3452, 0.3266) and eventually to reddish-orange (KNCP:0.008Eu^{2+}, 0.25Mn^{2+}) with CIE chromaticity coordinates of (0.4506, 0.3510) in the visible spectral region.

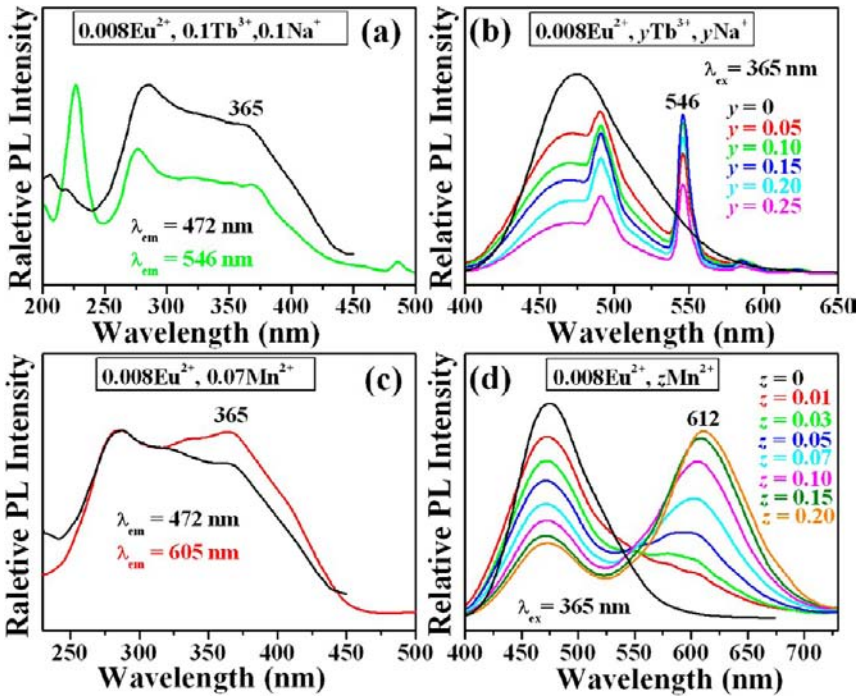

Figure 7. Excitation spectra for KNCP:0.008Eu^{2+}, 0.1Tb^{3+}, 0.1Na^{+} (a) and KNCP:0.008Eu^{2+}, 0.07Mn^{2+} (c) samples. The emission spectra for KNCP:0.008Eu^{2+}, yTb^{3+}, yNa^{+} (b) and KNCP:0.008Eu^{2+}, zMn^{2+} (d).

dx.doi.org/10.1021/ic402305x | Inorg. Chem. 2013, 52, 13708−13718

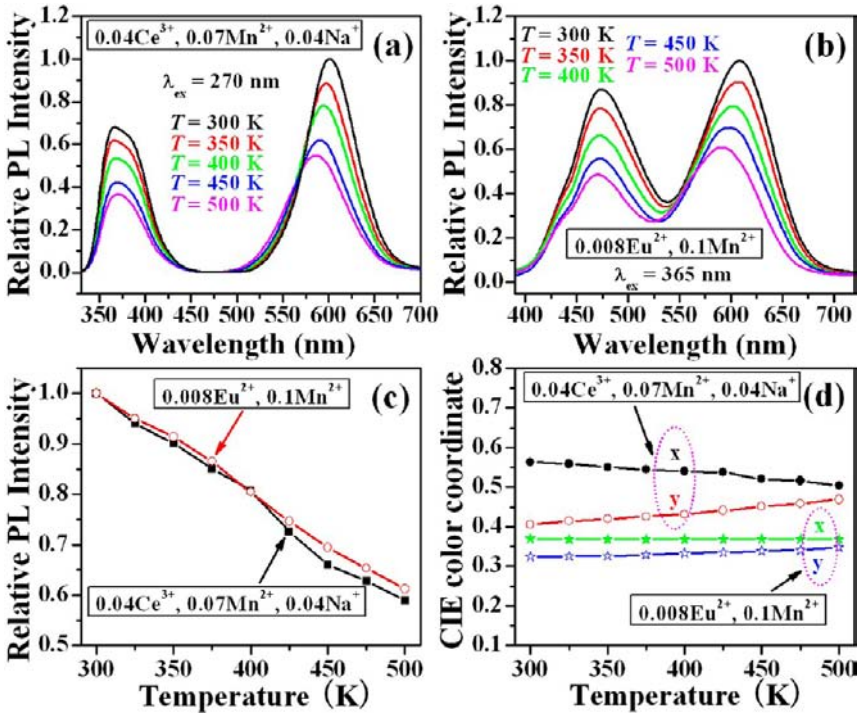

Figure 8. Selected temperature-dependent emission spectra of KNCP:0.04Ce^{3+}, 0.07Mn^{2+}, 0.04Na^{+} (a) and KNCP:0.008Eu^{2+}, 0.1Mn^{2+} (b) samples. Temperature-dependent integrated luminescence intensities (c) and CIE color coordinates (d) of KNCP:0.04Ce^{3+}, 0.07Mn^{2+}, 0.04Na^{+} and KNCP:0.008Eu^{2+}, 0.1Mn^{2+} phosphors.

The CIE chromaticity coordinates excited at 365 nm UV of KNCP:Eu^{2+}, Tb^{3+}/Mn^{2+}, Na^{+} phosphors with different Tb^{3+}/Mn^{2+} doping concentrations are depicted in Figure 6b. Table 1 lists the QYs of KNCP:Eu^{2+}, Tb^{3+}/Mn^{2+}, Na^{+} phosphors under 365 nm UV excitation. The QY of the KNCP:0.008Eu^{2+} phosphor is 57%, and the maximum QYs of KNCP:0.008Eu^{2+}, $y$$Tb^{3+}$, $y$$Na^{+}$ and KNCP:0.008Eu^{2+}, $z$$Mn^{2+}$ phosphors are 43% and 38% at y = 0.10 and z = 0.15, respectively. For the KNCP:Eu^{2+}, Tb^{3+}/Mn^{2+}, Na^{+} system, the excitation spectra range from 240 to 440 nm, which match well with current UV chips for LEDs. These results indicate that the KNCP:Eu^{2+}, Tb^{3+}/Mn^{2+}, Na^{+} phosphors could be regarded as potential candidates for UV LEDs.

3.4. Temperature Quenching. Thermal stability is one of the most important factors that should be taken into consideration when preparing phosphors for LEDs. That is because the luminescence intensity for most phosphors would decrease if the operation temperature exceeds some certain value due to temperature quenching effect.[28] Phosphors chosen for LEDs must sustain stable emission efficiency at temperatures of about 150 °C over a long term.[29] Figure 8a and b show selected temperature-dependent emission spectra of KNCP:0.04Ce^{3+}, 0.07Mn^{2+}, 0.04Na^{+} and KNCP:0.008Eu^{2+}, 0.1Mn^{2+} samples. The profiles of the emission spectra for the two samples are almost unchanged despite the fact that the temperature increases (T = 300−500 K). Figure 8c plots the temperature-dependent integrated luminescence intensities of the phosphors for investigation. The emission intensities decrease with an increase in temperature. However, the thermal quenching temperatures ($T_{0.5}$, defined as the temperature at which the emission intensity is 50% of its original value) for these two samples are both higher than 500 K. The results suggest that KNCP:0.04Ce^{3+}, 0.07Mn^{2+}, 0.04Na^{+} and KNCP:0.008Eu^{2+}, 0.1Mn^{2+} phosphors have good thermal stability against the temperature quenching effect. The following equation can be used to describe the relationship between the temperature and luminescence intensity:[30]

$$I_T = I_0\left[1 + c\,\exp\left(-\frac{\Delta E}{kT}\right)\right]^{-1} \quad (4)$$

where I_0 is the initial emission intensity, I_T is the intensity at different temperatures, c is a constant for a certain host, ΔE is the activation energy, k is the Boltzmann constant (8.629×10^{-5} eV·K^{-1}), and T is temperature. Figure 9 shows the plots of $-\ln[(I_0/I_T) - 1]$ versus $1/kT$ for KNCP:0.04Ce^{3+}, 0.07Mn^{2+}, 0.04Na^{+} (a) and KNCP:0.008Eu^{2+}, 0.1Mn^{2+} (b) samples. According to eq 4, the activation energy ΔE was calculated to be 0.197 eV for KNCP:0.04Ce^{3+}, 0.07Mn^{2+}, 0.04Na^{+} and 0.202 eV for KNCP:0.008Eu^{2+}, 0.1Mn^{2+}. In addition, the emission bands of Mn^{2+} in KNCP:0.04Ce^{3+}, 0.07Mn^{2+}, 0.04Na^{+} and KNCP:0.008Eu^{2+}, 0.1Mn^{2+} samples show a blue-shift with increasing temperature. A similar phenomenon has been found and studied in other Mn^{2+} ion doped phosphors.[31] The CIE chromaticity coordinates of KNCP:0.04Ce^{3+}, 0.07Mn^{2+}, 0.04Na^{+} and KNCP:0.008Eu^{2+}, 0.1Mn^{2+} samples at different temperatures are illustrated in Figure 8d. Clearly, the KNCP:0.008Eu^{2+}, 0.1Mn^{2+} sample has better color stability than that of the KNCP:0.04Ce^{3+}, 0.07Mn^{2+}, 0.04Na^{+} sample.

3.5. Cathodoluminescence Properties. Additionally, the CL properties of as-prepared KNCP:Ce^{3+}/Eu^{2+}/Sm^{3+}, Tb^{3+}/Mn^{2+}, Na^{+} phosphors have been investigated in detail. Figure 10 shows the typical CL spectra as well as the corresponding digital luminescence photographs of KNCP:Ce^{3+}/Eu^{2+}/Tb^{3+}/Mn^{2+}/Sm^{3+}, Na^{+} samples. Under low-voltage electron beam bombardment, the Ce^{3+}, Eu^{2+}, Tb^{3+}, Mn^{2+}, and Sm^{3+} ions give their characteristic emissions, respectively. The CL spectra are very similar to, but not identical with, their PL emissions

dx.doi.org/10.1021/ic402305x | Inorg. Chem. 2013, 52, 13708−13718

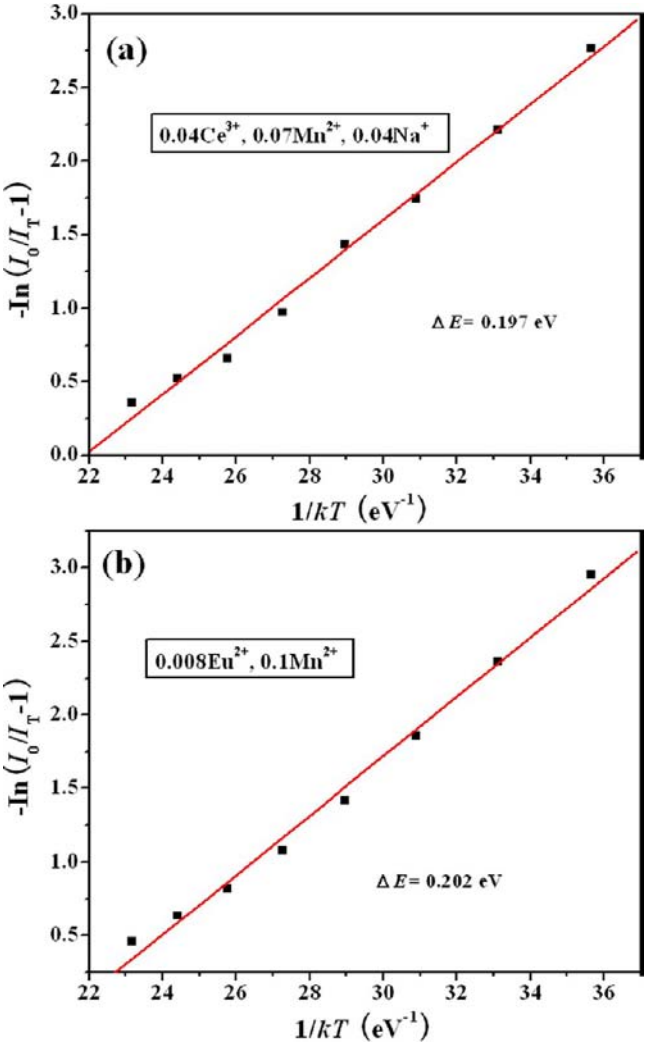

Figure 9. Plots of $-\ln[(I_0/I_T) - 1]$ versus $1/kT$ for KNCP:0.04Ce^{3+}, 0.07Mn^{2+}, 0.04Na^+ (a) and KNCP:0.008Eu^{2+}, 0.1Mn^{2+} (b) samples.

(Figure 2). For the KNCP:Mn^{2+} sample, the emission intensity of the high-energy band at 551 nm in the CL spectrum is higher than that in the PL spectrum. Similarly, the CL emission intensity of $^4G_{5/2} \rightarrow {}^6H_{5/2}$ (572 nm) and $^4G_{5/2} \rightarrow {}^6H_{7/2}$ transitions (600 nm) of Sm^{3+} increases compared with the PL intensity. A different excitation source is responsible for this observation.[32] For CL, the primary fast and energetic electrons create many secondary electrons with a very broad excitation energy distribution. So, all these electrons including primary and secondary electrons can populate not only the low-energy states but also the high-energy states of activators, yielding stronger high-energy emissions. The energy transfer properties of KNCP:Ce^{3+}/Eu^{2+}, Tb^{3+}/Mn^{2+}, Na^+ have been observed under low-voltage electron beam excitation. The CL emission spectra of KNCP:Ce^{3+}, Tb^{3+}/Mn^{2+}, Na^+ and KNCP:Eu^{2+}, Tb^{3+}/Mn^{2+}, Na^+ samples have similar properties to those of their PL spectra. With a fixed Ce^{3+}/Eu^{2+} concentration, the emission intensity of Ce^{3+}/Eu^{2+} decreases, while that of Tb^{3+}/Mn^{2+} gradually increases with increasing Tb^{3+}/Mn^{2+} concentration. Also, their CL colors can be tuned via energy transfer.

Similarly, the CL color of KNCP:*y*Tb^{3+}, *y*Na^+ samples can be adjusted from blue to green by changing the Tb^{3+}-doped concentration due to the cross-relaxation between $^5D_3$ and $^5D_4$ energy levels (see Figure S9 in the Supporting Information).

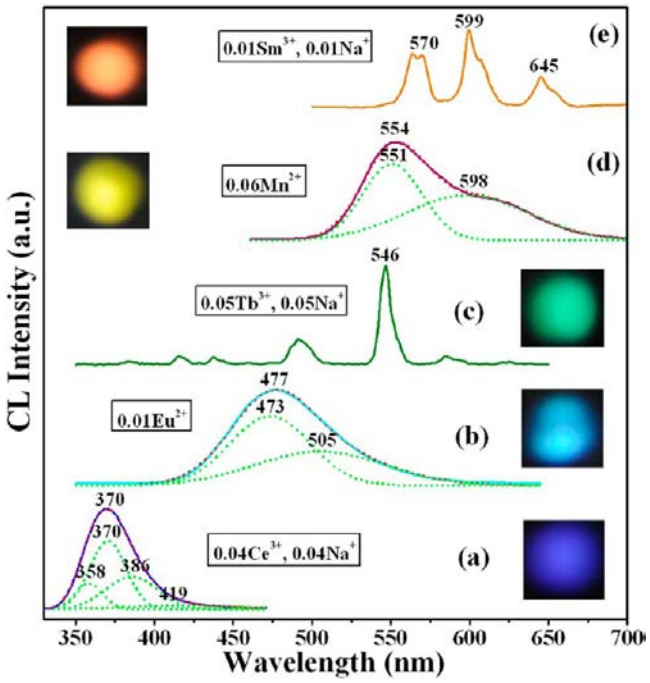

Figure 10. CL spectra for KNCP:0.04Ce^{3+}, 0.04Na^+ (a), KNCP:0.01Eu^{2+} (b), KNCP:0.05Tb^{3+}, 0.05Na^+ (c), KNCP:0.06Mn^{2+} (d), and KNCP:0.01Sm^{3+}, 0.01Na^+ (e). The insets display the corresponding digital luminescence photographs under low-voltage electron beam excitation.

Since KNCP:*y*Tb^{3+}, *y*Na^+ can give bluish-green emission at a suitable Tb^{3+} doping concentration and KNCP:*t*Sm^{3+}, *t*Na^+ shows reddish-orange emission under electron beam excitation, it is possible to achieve white light emission in the KNCP host by co-doping with Tb^{3+} and Sm^{3+} and adjusting their concentrations appropriately. Fortunately, the white light emission in the KNCP:Tb^{3+}, Sm^{3+}, Na^+ system has been obtained as expected. Figure 11 shows the CL spectra of KNCP:0.008Tb^{3+}, *t*Sm^{3+}, (0.008+*t*)Na^+, which contain the emission of both Tb^{3+} and Sm^{3+}. These emission spectra cover the entire visible light region with comparable intensity, resulting in white emission at t = 0.01. The CIE coordinates

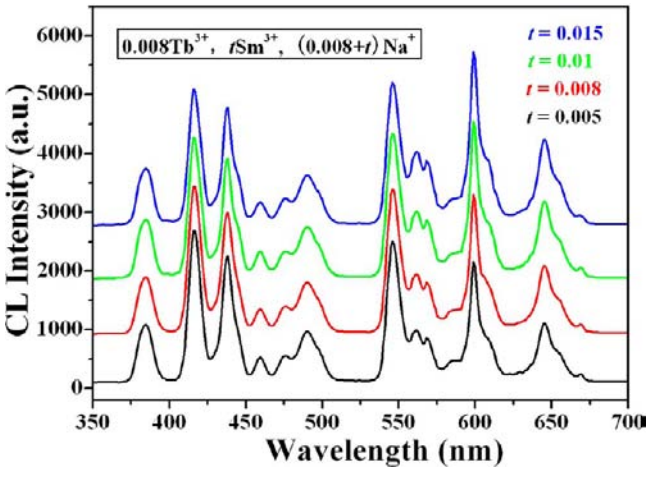

Figure 11. CL spectra for KNCP:0.008Tb^{3+}, *t*Sm^{3+}, (0.008+*t*)Na^+ under low-voltage electron beam excitation.

dx.doi.org/10.1021/ic402305x | *Inorg. Chem.* 2013, 52, 13708−13718

of KNCP:0.008Tb^{3+}, 0.01Sm^{3+}, 0.018Na^{+} (0.339, 0.3342) are very close to those of standard white light (0.33, 0.33).

Figure 12 shows the CL intensity of selected samples in the KNCP:Ce^{3+}/Eu^{2+}/Sm^{3+}, Tb^{3+}/Mn^{2+}, Na^{+} system as a function

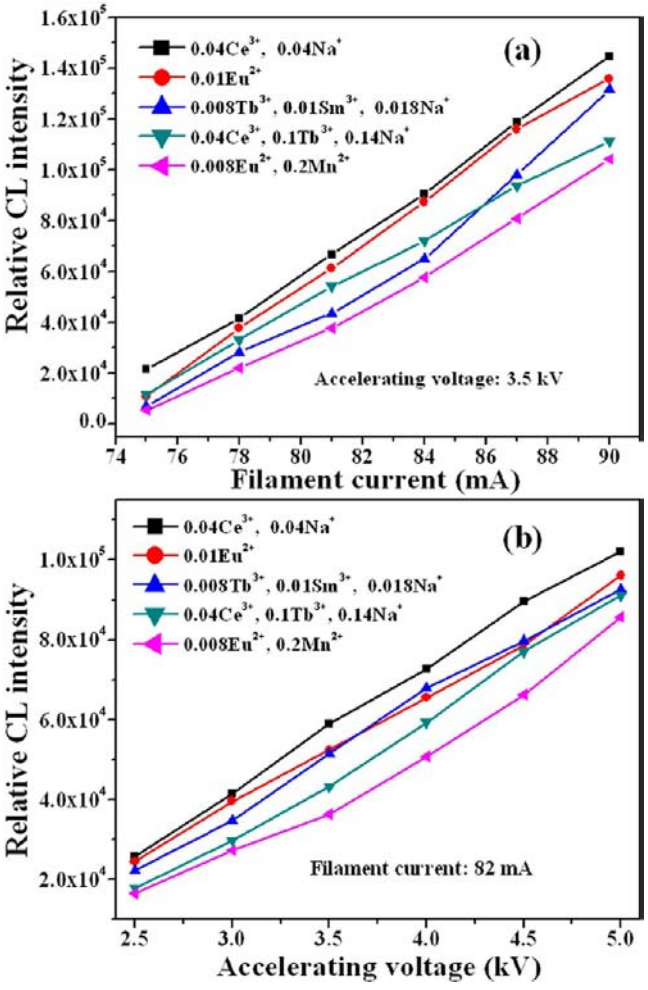

Figure 12. CL intensity of KNCP:0.04Ce^{3+}, 0.04Na^{+}, KNCP:0.01Eu^{2+}, KNCP:0.008Tb^{3+}, 0.01Sm^{3+}, 0.018Na^{+}, KNCP:0.04Ce^{3+}, 0.1Tb^{3+}, 0.14Na^{+}, and KNCP:0.008Eu^{2+}, 0.2Mn^{2+} samples as a function of filament current (a) and accelerating voltage (b).

of filament current and accelerating voltage. The CL intensities increase as filament current and accelerating voltage increase, which is attributed to the deeper penetration of the electrons into the phosphor, and thus more plasma will be produced, which results in more activator ions being excited. There is no obvious saturation effect observed for the CL at higher filament current and accelerating voltages.

4. CONCLUSION

In conclusion, the single-composition phosphors KNCP:A (A = Ce^{3+}, Eu^{2+}, Sm^{3+}, Tb^{3+}, Mn^{2+}) have been prepared by a Pechini-type sol–gel method. PL and CL properties of as-prepared phosphors were investigated in detail. Na^{+} ions were chosen as the charge compensators for Ce^{3+}-, Tb^{3+}-, and Sm^{3+}-doped KNCP phosphors. The energy transfers from Ce^{3+} to Tb^{3+} and Mn^{2+} ions as well as from Eu^{2+} to Tb^{3+} and Mn^{2+} have been validated by the emission spectra, PL decay, and the energy transfer efficiencies. The KNCP:Ce^{3+}/Eu^{2+}, Tb^{3+}/Mn^{2+}, Na^{+} samples show wide-range-tunable blue, green, reddish-orange, and white emissions under UV and low-voltage electron beam excitation. Due to the cross-relaxation from $^5D_3$ to $^5D_4$, the KNCP:Tb^{3+}, Na^{+} sample shows tunable luminescence from blue to cyan and then to green with the change of Tb^{3+}-doping concentration. A white emission can also be obtained under low-voltage electron beam excitation by co-doping Tb^{3+} and Sm^{3+} ions into the single-phase KNCP host. Additionally, the temperature-dependent PL properties of as-prepared phosphors demonstrate that the KNCP host has good thermal stability. The activation energy (ΔE) was calculated to be 0.197 eV for KNCP:0.04Ce^{3+}, 0.07Mn^{2+}, 0.04Na^{+} and 0.202 eV for KNCP:0.008Eu^{2+}, 0.1Mn^{2+}. In a word, the KNCP:A (A = Ce^{3+}, Eu^{2+}, Sm^{3+}, Tb^{3+}, Mn^{2+}) phosphors could be regarded as potential candidates for UV LEDs and FEDs.

■ ASSOCIATED CONTENT

Supporting Information

Diffuse reflection spectra of KNCP, KNCP:0.04Ce^{3+}, 0.04Na^{+}, KNCP:0.01Eu^{2+}, KNCP:0.05Tb^{3+}, 0.05Na^{+}, KNCP:0.06Mn^{2+}, and KNCP:0.01Sm^{3+}, 0.01Na^{+} samples (Figure S1); energy level diagrams of Ce^{3+}, Eu^{2+}, and Mn^{2+} at two different coordination fields (Figure S2); emission spectra for KNCP:0.02Ce^{3+}, M (a) and KNCP:0.05Tb^{3+}, M (M = Li^{+}, Na^{+}, and K^{+}) (b) (Figure S3); relative emission intensities for KNCP:*x*Ce^{3+}, *x*Na^{+} (a), KNCP:*m*Eu^{2+} (b), KNCP:*z*Mn^{2+} (c), and KNCP:*t*Sm^{3+}, *t*Na^{+} samples (d) with respect to the concentration of activators (Figure S4); comparison of the PL intensity of KNCP:Tb^{3+}/Mn^{2+}, Na^{+} with that of KNCP:Ce^{3+}, Tb^{3+}/Mn^{2+}, Na^{+} phosphors (a and b) and KNCP:Eu^{2+}, Tb^{3+}/Mn^{2+}, Na^{+} phosphors (c and d) (Figure S5); relative emission intensity of Ce^{3+}, Tb^{3+}, and Mn^{2+} in KNCP:0.04Ce^{3+}, *y*Tb^{3+}, (0.04+*y*)Na^{+} (a) and KNCP:0.04Ce^{3+}, *z*Mn^{2+}, 0.04Na^{+} (b) samples with different Tb^{3+}/Mn^{2+} doping concentrations (Figure S6); relative emission intensity of Eu^{2+}, Tb^{3+}, and Mn^{2+} in KNCP:0.008Eu^{2+}, *y*Tb^{3+}, *y*Na^{+} (a) and KNCP:0.008Eu^{2+}, *z*Mn^{2+} (b) samples with different Tb^{3+}/Mn^{2+} doping concentrations (Figure S7); decay curves for the luminescence of Eu^{2+} in KNCP:0.008Eu^{2+}, *y*Tb^{3+}, *y*Na^{+} (a) and KNCP:0.008Eu^{2+}, *z*Mn^{2+} (c) samples with different Tb^{3+}/Mn^{2+} doping concentrations; dependence of the energy transfer efficiency η on *y* (b) and *z* (d) (Figure S8); CL spectra for KNCP:*y*Tb^{3+}, *y*Na^{+} under low-voltage electron beam excitation (Figure S9). This information is available free of charge via the Internet at http://pubs.acs.org.

■ AUTHOR INFORMATION

Corresponding Author

*E-mail: jlin@ciac.ac.cn (Jun Lin).

Notes

The authors declare no competing financial interest.

■ ACKNOWLEDGMENTS

This project is financially supported by National Basic Research Program of China (2010CB327704) and the National Natural Science Foundation of China (NSFC 51172227, 51332008, 21221061), and the Joint Funds of the National Natural Science Foundation of China and Guangdong Province (Grant No. U13012038).

■ REFERENCES

(1) (a) Roh, H.-S.; Kim, D. H.; Park, I.-J.; Song, H. J.; Hur, S.; Kim, D.-W.; Hong, K. S. *J. Mater. Chem.* **2012**, *22*, 12275–12280. (b) Xia,

Z.; Zhuang, J.; Liao, L. *Inorg. Chem.* **2012**, *51*, 7202−7209. (c) Jing, H.; Guo, C.; Zhang, G.; Su, X.; Yang, Z.; Jeong, J. H. *J. Mater. Chem.* **2012**, *22*, 13612−13618. (d) Hao, J.; Cocivera, M. *Appl. Phys. Lett.* **2001**, *79*, 740. (e) Liu, T.-C.; Kominami, H.; Greer, H. F.; Zhou, W.; Nakanishi, Y.; Liu, R.-S. *Chem. Mater.* **2012**, *24*, 3486−3492. (f) Liu, C.; Zhang, S.; Liu, Z.; Liang, H.; Sun, S.; Tao, Y. *J. Mater. Chem. C* **2013**, *1*, 1305−1308. (g) Raju, G. S. R.; Park, J. Y.; Jung, H. C.; Pavitra, E.; Moon, B. K.; Jeong, J. H.; Kim, J. H. *J. Mater. Chem.* **2011**, *21*, 6136−6139.

(2) (a) Hsu, C.-H.; Das, S.; Lu, C.-H. *J. Electrochem. Soc.* **2012**, *159*, J193−J199. (b) Kulshreshtha, C.; Kwak, J. H.; Park, Y.-J.; Sohn, K.-S. *Opt. Lett.* **2009**, *34*, 794−796. (c) Li, X.; Budai, J. D.; Liu, F.; Howe, J. Y.; Zhang, J.; Wang, X.-J.; Gu, Z.; Sun, C.; Meltzer, R. S.; Pan, Z. *Light: Sci. Appl.* **2013**, *2*, e50.

(3) (a) Wu, L.; Zhang, Y.; Gui, M.; Lu, P.; Zhao, L.; Tian, S.; Kong, Y.; Xu, J. *J. Mater. Chem.* **2012**, *22*, 6463−6470. (b) Liu, Y.; Zhang, X.; Hao, Z.; Wang, X.; Zhang, J. *Chem. Commun.* **2011**, *47*, 10677−10679. (c) Xie, R. J.; Hirosaki, N.; Kimura, N.; Sakuma, K.; Mitomo, M. *Appl. Phys. Lett.* **2007**, *90*, 191101. (d) Wu, Y.-C.; Chen, Y.-C.; Wang, D.-Y.; Lee, C.-S.; Sun, C.-C.; Chen, T.-M. *J. Mater. Chem.* **2011**, *21*, 15163−15166. (e) Su, S.; Liu, W.; Duan, R.; Cao, L.; Su, G.; Zhao, C. *J. Alloys Compd.* **2013**, *575*, 309−313.

(4) (a) Huang, C. H.; Chen, T. M. *J. Phys. Chem. C* **2011**, *115*, 2349−2355. (b) Kim, M. S.; Bharat, L. K.; Yu, J. S. *J. Lumin.* **2013**, *142*, 92−95.

(5) (a) Hao, J. H.; Gao, J. *Appl. Phys. Lett.* **2004**, *85*, 3720. (b) Ghoul, J. E.; Omri, K.; Alyamani, A.; Barthou, C.; Mir, L. E. *J. Lumin.* **2013**, *138*, 218−222. (c) Shang, M.; Geng, D.; Yang, D.; Kang, X.; Zhang, Y. *Inorg. Chem.* **2013**, *52*, 3102−3112.

(6) (a) Del Toro, R.; Hernandez, P.; Diaz, Y.; Brito, J. L. *Mater. Lett.* **2013**, *107*, 231−234. (b) Geng, D.; Shang, M.; Yang, D.; Zhang, Y.; Cheng, Z.; Lin, J. *Dalton Trans.* **2012**, *41*, 14042−14045. (c) Liu, X.; Lin, J. *J. Mater. Chem.* **2008**, *18*, 221−228.

(7) Lin, J.; Yu, M.; Lin, C.; Liu, X. *J. Phys. Chem. C* **2007**, *111*, 5835−5845.

(8) Wang, Z.-J.; Li, Y.; Wang, Y.; Li, P.-L.; Guo, Q.-L.; Wang, Z.-P. *J. Inorg. Mater.* **2011**, *26*, 731−734.

(9) (a) Birkel, A.; Denault, K. A.; George, N. C.; Doll, C. E.; Héry, B.; Mikhailovsky, A. A.; Birkel, C. S.; Hong, B.-C.; Seshadri, R. *Chem. Mater.* **2012**, *24*, 1198−1204. (b) Qu, X.; Yang, H. K.; Pan, G.; Chung, J. W.; Moon, B. K.; Choi, B. C.; Jeong, J. H. *Inorg. Chem.* **2011**, *50*, 3387−3393.

(10) (a) Duan, C.; Zhang, Z.; Rösler, S.; Rösler, S.; Delsing, A.; Zhao, J.; Hintzen, H. T. *Chem. Mater.* **2011**, *23*, 1851−1861. (b) Shang, M.; Li, G.; Geng, D.; Yang, D.; Kang, X.; Zhang, Y.; Lian, H.; Lin, J. *J. Phys. Chem. C* **2012**, *116*, 10222−10231.

(11) Van Uitert, L. G. *J. Lumin.* **1984**, *29*, 1−9.

(12) (a) Yan, X.; Li, W.; Sun, K. *J. Alloys Compd.* **2010**, *508*, 475−479. (b) Wang, Z.; Li, P.; Zhang, X.; Li, Q.; Li, T.; Yang, Z.; Guo, Q. *Phys. B (Amsterdam, Neth.)* **2013**, *414*, 56−59.

(13) (a) Li, Y.-C.; Chang, Y.-H.; Lin, Y.-F.; Lin, Y.-J.; Chang, Y.-S. *Appl. Phys. Lett.* **2006**, *89*, 081110. (b) Grzyb, T.; Lis, S. *Inorg. Chem.* **2011**, *50*, 8112−8120. (c) Inaguma, Y.; Muronoi, T.; Sano, K.; Tsuchiya, T.; Mori, Y.; Katsumata, T.; Mori, D. *Inorg. Chem.* **2011**, *50*, 5389−5395. (d) Zhu, L.; Lu, A.; Zuo, C.; Shen, W. *J. Alloys Compd.* **2011**, *509*, 7789−7793.

(14) Li, G.; Geng, D.; Shang, M.; Peng, C.; Cheng, Z.; Lin, J. *J. Mater. Chem.* **2011**, *21*, 13334−13344.

(15) (a) Guo, N.; Song, Y.; You, H.; Jia, G.; Yang, M.; Liu, K.; Zheng, Y.; Huang, Y.; Zhang, H. *Eur. J. Inorg. Chem.* **2010**, 4636−4642. (b) Geng, D.; Li, G.; Shang, M.; Yang, D.; Zhang, Y.; Cheng, Z.; Lin, J. *J. Mater. Chem.* **2012**, *22*, 14262−14271.

(16) (a) Ricci, P. C.; Carbonaro, C. M.; Corpino, R.; Cannas, C.; Salis, M. *J. Phys. Chem. C* **2011**, *115*, 16630−16636. (b) Xie, M.; Tao, Y.; Huang, Y.; Liang, H.; Su, Q. *Inorg. Chem.* **2010**, *49*, 11317−11324. (c) Kumar, M.; Seshagiri, T. K.; Kadam, R. M.; Godbole, S. V. *Mater. Res. Bull.* **2011**, *46*, 1359−1365.

(17) (a) Sohn, K.-S.; Choi, Y. Y.; Park, H. D.; Choi, Y. G. *J. Electrochem. Soc.* **2000**, *147*, 2375−2379. (b) Sohn, K.-S.; Shin, N. *Electrochem. Solid-State Lett.* **2002**, *5*, H21−H23.

(18) (a) Costa, G. K. B.; Pedro, S. S.; Carvalho, I. C. S.; Sosman, L. P. *Opt. Mater.* **2009**, *31*, 1620−1627. (b) Xu, M. J.; Wang, L. X.; Jia, D. Z.; Liu, L.; Zhang, L.; Guo, Z. P.; Sheng, R. *J. Am. Ceram. Soc.* **2013**, *96*, 1198−1202.

(19) (a) Jeong, J.; Bandi, V. R.; Grandhe, B. K.; Jang, K.; Lee, H. S.; Yi, S. S.; Jeong, J. H. *J. Korean Phys. Soc.* **2011**, *58*, 306−310. (b) Kang, D.; Yoo, H. S.; Jung, S. H.; Kim, H.; Jeon, D. Y. *J. Phys. Chem. C* **2011**, *115*, 24334−24340.

(20) (a) Chen, M.; Xie, L.; Li, F.; Zhou, S.; Wu, L. *ACS Appl. Mater. Interfaces* **2010**, *2*, 2733−2737. (b) Boyer, J.-C.; Gagnon, J.; Cuccia, L. A.; Capobianco, J. A. *Chem. Mater.* **2007**, *19*, 3358−3360. (c) Liu, Y.; Zhang, X.; Hao, Z.; Luo, Y.; Wang, X.; Zhang, J. *J. Mater. Chem.* **2011**, *21*, 16379−16384.

(21) Zhang, Q.; Wang, J.; Zhang, G.; Su, Q. *J. Mater. Chem.* **2009**, *19*, 7088−7092.

(22) (a) Yu, M.; Lin, J.; Fang, J. *Chem. Mater.* **2005**, *17*, 1783−1791. (b) Liu, Y.; Hao, J.; Zhuang, W.; Hu, Y. *J. Phys. D: Appl. Phys.* **2009**, *42*, 245102.

(23) (a) Kwon, K. H.; Im, W. B.; Jang, H. S.; Yoo, H. S.; Jeon, D. Y. *Inorg. Chem.* **2009**, *48*, 11525−11532. (b) Sinha, G.; Patra, A. *Chem. Phys. Lett.* **2009**, *473*, 151−154. (c) Mandal, S.; Bhattacharyya, S.; Borovkov, V.; Patra, A. *J. Phys. Chem. C* **2012**, *116*, 11401−11407. (d) Zhu, Y.; Sun, Z.; Yin, Z.; Song, H.; Xu, W.; Wang, Y.; Zhang, L.; Zhang, H. *Dalton Trans.* **2013**, *42*, 8049−8057. (e) Ruan, Y.; Xiao, Q.; Luo, W.; Li, R.; Chen, X. *Nanotechnology* **2011**, *22*, 275701.

(24) (a) Ghosh, P.; Kar, A.; Patra, A. *Nanoscale* **2010**, *2*, 1196−1202. (b) Liu, W.-R.; Chiu, Y.-C.; Yeh, Y.-T.; Jang, S.-M.; Chen, T.-M. *J. Electrochem. Soc.* **2009**, *156*, J165−J169.

(25) Tang, W.; Fu, T.; Deng, K.; Wu, M. *Ceram. Int.* **2013**, *39*, 6363−6367.

(26) Dai, P.; Zhang, X.; Bian, L.; Lu, S.; Liu, Y.; Wang, X. *J. Mater. Chem. C* **2013**, *1*, 4570−4576.

(27) Liu, W.-R.; Huang, C.-H.; Yeh, C.-W.; Chiu, Y.-C.; Yeh, Y.-T.; Liu, R.-S. *RSC Adv.* **2013**, *3*, 9023−9028.

(28) (a) Dutczak, D.; Ronda, C.; Meijerink, A.; Jüstel, T. *J. Lumin.* **2013**, *141*, 150−154. (b) Bachmann, V.; Ronda, C.; Oeckler, O.; Schnick, W.; Meijerink, A. *Chem. Mater.* **2009**, *21*, 316−325.

(29) (a) Xie, R.-J.; Hirosaki, N.; Suehiro, T.; Xu, F.-F.; Mitomo, M. *Chem. Mater.* **2006**, *18*, 5578−5583. (b) Yeh, C.-W.; Chen, W.-T.; Liu, R.-S.; Hu, S.-F.; Sheu, H.-S.; Chen, J.-M.; Hintzen, H. T. *J. Am. Chem. Soc.* **2012**, *134*, 14108−14117. (c) Krings, M.; Montana, G.; Dronskowski, R.; Wickleder, C. *Chem. Mater.* **2011**, *23*, 1694−1699.

(30) (a) Huang, Y.; Nakai, Y.; Tsuboi, T.; Seo, H. J. *Opt. Express* **2011**, *19*, 6303−6311. (b) Orive, J.; Balda, R.; Fernández, J.; Lezama, L.; Arriortua, M. *Dalton Trans.* **2013**, *42*, 12481−12494.

(31) (a) Zhang, X.; Gong, M. *Mater. Lett.* **2011**, *65*, 1756−1758. (b) Liu, W.-R.; Huang, C.-H.; Yeh, C.-W.; Tsai, J.-C.; Chiu, Y.-C.; Yeh, Y.-T.; Liu, R.-S. *Inorg. Chem.* **2012**, *51*, 9636−9641.

(32) (a) Geng, D.; Shang, M.; Yang, D.; Zhang, Y.; Cheng, Z.; Lin, J. *J. Mater. Chem.* **2012**, *22*, 23789−23798. (b) Zhu, G.; Ci, Z.; Wang, Q.; Wen, Y.; Han, S.; Shi, Y.; Xin, S.; Wang, Y. *J. Mater. Chem. C* **2013**, *1*, 4490−4496. (c) Li, G.; Zhang, Y.; Geng, D.; Shang, M.; Peng, C.; Cheng, Z.; Lin, J. *ACS Appl. Mater. Interfaces* **2012**, *4*, 296−305.